

## Evidence for the isovector giant quadrupole resonance in $^{16}\text{O}$ from the $^{16}\text{O}(\gamma, n_0)^{15}\text{O}$ reaction

T. W. Phillips and R. G. Johnson\*

Lawrence Livermore Laboratory, University of California, Livermore, California 94550

(Received 26 June 1979)

The cross section and angular distribution for the reaction  $^{16}\text{O}(\gamma, n_0)^{15}\text{O}$  have been measured over an excitation energy range of 25–45 MeV. Neutron time-of-flight spectra were recorded at six angles (22.5°, 45°, 67.5°, 90°, 112.5°, and 135°) and at four bremsstrahlung end-point energies (30, 35, 40, and 45 MeV). Differential cross sections deduced from these spectra were fitted by a fourth-order Legendre-polynomial expansion. The cross section obtained from this expansion decreases smoothly from 3.95 mb at 25.5 MeV to 0.22 mb at 43.8 MeV. The appearance in this analysis of large first-, third-, and especially fourth-order coefficients, is strong evidence for significant  $E2$  cross section. An  $E2$  cross section extracted from the data exhausts approximately 68% of the isovector  $E2$  energy-weighted sum rule. The present data are compared to previous related measurements and excellent agreement is seen. In comparisons with theoretical studies on  $^{16}\text{O}$ , there is good general agreement but relatively poor detailed agreement.

[ NUCLEAR REACTIONS  $^{16}\text{O}(\gamma, n_0)^{15}\text{O}$ ,  $E_x = 25\text{--}45$  MeV; measured  $\sigma(E_x, \theta)$ ; deduced  $E2$  strength. ]

### I. INTRODUCTION

The existence of giant resonances of multipolarity other than  $E1$  (i.e.,  $M1$ ,  $E2$ ,  $E3$ ) has been well established for medium-weight and heavy nuclei primarily by inelastic electron and hadron scattering experiments.<sup>1</sup> In light nuclei the evidence for higher multipole resonances is not nearly as complete. For example, in  $^{16}\text{O}$ , where the  $E1$  giant resonance (GDR) has been extensively studied, the isoscalar ( $\Delta T = 0$ )  $E2$  giant resonance ( $\text{GQR}_0$ ), although elusive, has apparently been found by inelastic alpha (Ref. 2), ( $p, \gamma_0$ ) (Ref. 3), and electron (Ref. 4) studies. This resonance is centered at approximately 20 MeV, and although its strength is considerably spread out, it exhausts a major fraction of the isoscalar energy-weighted sum rule ( $\text{EWSR}_0$ ). On the other hand, very little experimental evidence has been obtained for the isovector ( $\Delta T = 1$ )  $E2$  giant resonance ( $\text{GQR}_1$ ). Because light nuclei, especially closed-shell nuclei, are perhaps the best understood in terms of microscopic theories, it is quite important that the experimental data be complete. Consequently the present search for the  $\text{GQR}_1$  in  $^{16}\text{O}$  was undertaken, using the  $^{16}\text{O}(\gamma, n_0)^{15}\text{O}$  reaction as a probe.

Since isoscalar modes of oscillation are generally pushed down in energy from their unperturbed positions, and isovector modes are pushed up in energy, the  $\text{GQR}_1$  should appear above the GDR. In the simplest shell model description  $E2$  absorption is characterized by the excitation of particles from closed shells to orbitals two units higher in the major quantum number, i.e.,  $2\hbar\omega$  transitions. This would place the unperturbed  $E2$  giant resonance at approximately 28 MeV in  $^{16}\text{O}$ .

More sophisticated microscopic theories place the  $\text{GQR}_1$  at anywhere from 30 to 50 MeV.<sup>5</sup> In addition, considerable spreading of the strength is expected at these excitation energies. The present experiment was designed to study excitation energies in the range of 25 to 45 MeV and to test for the presence of  $E2$  absorption by measuring the angular distribution of ground-state photoneutrons.

Much of the experimental investigation of this region has been done using the  $^{15}\text{N}(p, \gamma_0)^{16}\text{O}$  reaction.<sup>6-10</sup> The results of these measurements, in particular those of Refs. 8 and 10 which reach excitation energies near 40 MeV, are consistent with considerable  $E2$  strength in the 30 to 50 MeV region. Unfortunately the interpretation of the ( $p, \gamma_0$ ) reaction has not been straightforward because direct capture and resonant capture cannot be separated. Since the proton has a large recoil effective quadrupole charge while that of the neutron is very small,<sup>11</sup> there will be little direct capture in the neutron channel. This experiment provides a test of these assumptions.

Experiments using other reactions, in particular inelastic alpha scattering and alpha particle capture<sup>2</sup> and electron scattering,<sup>4</sup> have been done which included this energy region but make no statement about  $E2$  strength. In the case of the alpha scattering experiment, it would be expected that isoscalar modes are preferentially excited. The electron scattering experiment is apparently not sensitive enough in the 30 to 50 MeV region to separate higher multipole strength from underlying  $E1$  strength. In another experiment using inelastic scattering of polarized protons,<sup>12</sup> not only was considerable  $E2$  strength obtained but an  $E3$  (presumably isoscalar) resonance was seen centered at

about 35 MeV. These data will be examined more fully below.

Theoretically there are several microscopic treatments of higher multipole photoabsorption in  $^{16}\text{O}$  (Refs. 13–18). Among the more detailed is the work of Liu and Brown<sup>16</sup> which predicts giant resonances from monopole through hexadecapole for  $^{16}\text{O}$ ,  $^{40}\text{Ca}$ ,  $^{90}\text{Zr}$ , and  $^{208}\text{Pb}$ . Other studies by Heil<sup>17</sup> and Marangoni *et al.*<sup>15</sup> predict both cross sections and angular distributions which will be especially important to the present measurement.

The measurement reported here is a study of the  $^{16}\text{O}(\gamma, n_0)^{15}\text{O}$  cross section and neutron angular distribution. Neutron time-of-flight spectra were collected at six laboratory angles ( $22.5^\circ$ ,  $45^\circ$ ,  $67.5^\circ$ ,  $90^\circ$ ,  $112.5^\circ$ , and  $135^\circ$ ) and at four bremsstrahlung end-point energies (30, 35, 40, and 45 MeV). From the differential cross sections the coefficients of a fourth-order Legendre polynomial expansion were extracted. Under the assumption that  $M1$  absorption is small, evidence for  $E2$  strength would be obtained by the observation of nonzero first-, third-, and fourth-order coefficients.

## II. EXPERIMENTAL PROCEDURE

The experiment was performed at the Lawrence Livermore Laboratory 100 MeV Electron-Positron Linear Accelerator, using the bremsstrahlung-induced neutron time-of-flight technique. Since this facility for measuring photoneutron cross sections and angular distributions has not been described previously, some details will be presented. On the other hand, the techniques used are in general standard, so that full details of all aspects of the experiment are unnecessary.

### A. Data Acquisition

An overview of the experimental apparatus is shown in Fig. 1. An energy-analyzed pulsed beam of electrons (with a 2% momentum spread) from the linear accelerator was focused on a thin bremsstrahlung converter (a  $1.27 \times 10^{-2}$ -mm thick gold foil). The beam pulse had a width of 5 ns and a repetition rate of 1440 pulses per second. Electrons passing through the converter were magnetically deflected vertically down into a 5-m deep beam dump. At the bottom of the beam dump an aluminum block stopped the beam and the charge collected on the block was integrated and scaled. The bremsstrahlung beam produced at the converter was incident on a photonuclear sample which sat on a light aluminum stand at the intersection of the time-of-flight lines. The photonuclear samples were attached to a remotely controlled sample changing system (with a capacity of

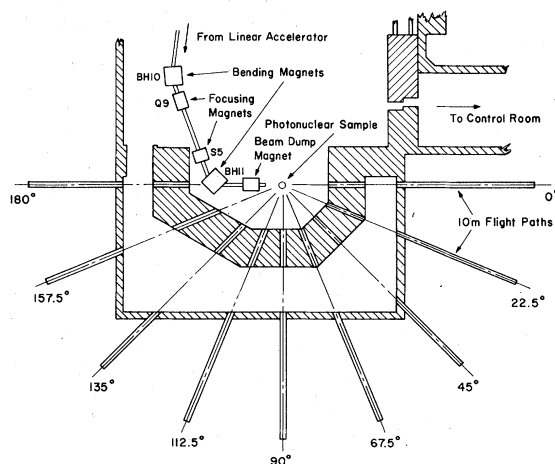


FIG. 1. Schematic diagram of the facility for photoneutron cross section and angular-distribution measurements at Lawrence Livermore Laboratory. An insertable bremsstrahlung converter preceded the beam dump magnet and neutron detectors were placed at the ends of the 10-m flight paths.

5 samples) attached to the ceiling. Samples used in this study were 534 g of  $\text{H}_2\text{O}$ , 788 g of  $\text{D}_2\text{O}$ , 679 g of  $\text{CH}_2$ , 2.02 kg of depleted uranium, and an empty sample container. All samples were packaged in thin walled (0.03-mm thick) cylindrical aluminum containers whose dimensions were 5.1 cm (radius) by 10.2 cm (height). In order to reduce neutron scattering in the  $\text{H}_2\text{O}$  sample, its container (and the empty sample container) was chosen to be an annular cylinder with an inner radius of 2.5 cm and the same outer dimensions as above.

Neutrons emitted by a sample were detected at the end of 10-m flight paths by proton-recoil neutron detectors. In order to decrease gamma flash, lead filters ranging in thickness from 0.64 to 3.8 cm were put in each flight path. Each neutron detector [illustrated in Fig. 2(a)] consisted of three 5.1-cm (or 12.7-cm) thick by 12.7-cm diameter plastic scintillators (Pilot-B) each viewed by two 12.7-cm diameter photomultiplier tubes (RCA-8854 or RCA-4522). The overall time resolution of the experiment was 6 ns.

A block diagram of the data acquisition system is shown in Fig. 2(b). In this figure the electronics for one of the six detectors is shown in the indicated area. Anode signals from each photomultiplier tube are routed to a discriminator set at a 50-mV threshold to reduce the response to photomultiplier noise. In order to further eliminate response to noise, a coincidence between each pair of photomultipliers on a single scintillator was required. A valid signal from any of the three

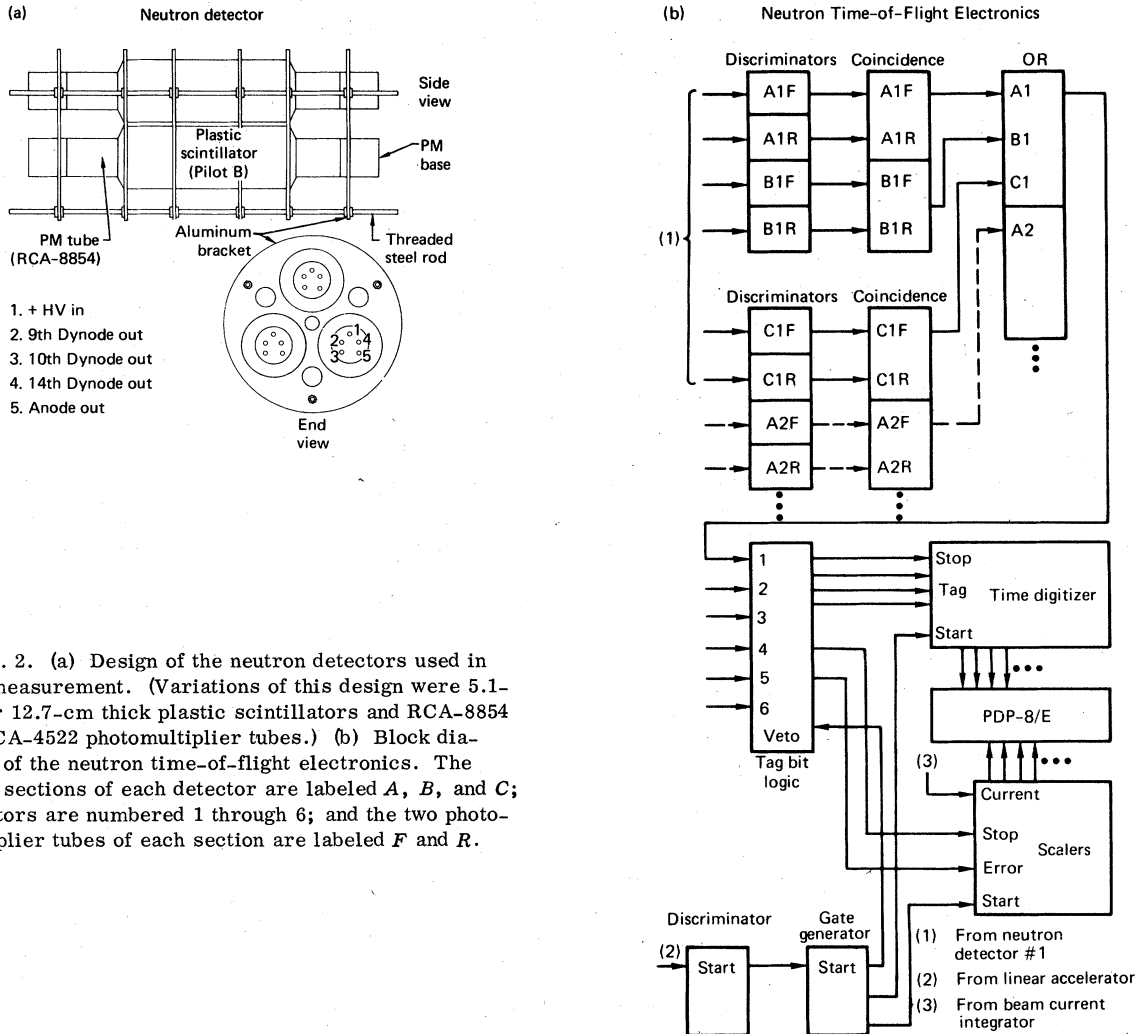


FIG. 2. (a) Design of the neutron detectors used in this measurement. (Variations of this design were 5.1-cm or 12.7-cm thick plastic scintillators and RCA-8854 or RCA-4522 photomultiplier tubes.) (b) Block diagram of the neutron time-of-flight electronics. The three sections of each detector are labeled *A*, *B*, and *C*; detectors are numbered 1 through 6; and the two photomultiplier tubes of each section are labeled *F* and *R*.

sections of each detector is passed through a circuit which generates a single output pulse for one or more input pulses. Logic signals from each detector are then sent through a series of circuits [shown as one box in Fig. 2(b)] which provided a single stop pulse and a three bit tag identifying the detector for that stop pulse. Also shown is an input which gated the circuit off during the gamma flash. Stop pulses and tags were then routed to the time digitizer (EGG-TDC-100) which was set at 2-ns time channels. The start pulse for the time digitizer was obtained from a fast toroidal transformer mounted between the first and second sections of the linear accelerator. The time-of-flight data were then read into a PDP 8/E computer and stored in six separate 1536-channel arrays. The computer also controlled a set of scalars which recorded the number of beam pulses (starts), the total number of events detected (stops), and the scaled current from the dump

block.

Neutron time-of-flight spectra at six angles from  $22.5^\circ$  through  $135^\circ$  in  $22.5^\circ$  steps and at four electron end-point energies from 30- through 45- in 5-MeV steps were accumulated for each of the samples. In addition spectra for the depleted uranium sample with 10.2-cm graphite filters in each flight path were also taken (to test the neutron energy calibration, using the absorption resonances in  $^{12}\text{C}$ ).

#### B. Data Analysis

The data analysis for the  $^{16}\text{O}$  spectra can be considered as a three stage process. Initial corrections were performed on the time-of-flight spectra. Secondly, the spectra were converted to neutron energy spectra and additional corrections were made. Finally, conversion to spectra as a function of excitation energy (assuming ground-state

neutron transitions) was carried out. Following further corrections at this stage, cross sections and angular distributions were extracted. These stages of analysis are described in detail below.

Since the data were taken with a single time digitizer and a tag indicating the detector, there was the possibility that for each beam pulse, events appearing in more than one detector would set an incorrect tag. In addition, there was the usual problem of dead time, i.e., more than one event in the same detector for a given beam pulse. At the data rate in this experiment, the probability of either of these occurrences was small (approximately 15%) and corrections for both effects were subsequently made. It is estimated that this correction makes at most a 1.5% contribution to the systematic error in the time-of-flight spectra at any angle.

For each time-of-flight spectrum the following backgrounds were removed: (1) time-independent background due to photomultiplier noise, cosmic rays, and other natural backgrounds, (2) a background due to a slowly decaying portion of the gamma flash, and (3) neutron background from photoneutron reactions in the aluminum sample container. A typical time-of-flight spectrum (in this case for a 45-MeV end point and an angle of 68°) is shown in Fig. 3 with the backgrounds indi-

cated. Time-independent backgrounds were obtained from time-of-flight regions which were equivalent to neutron energies below the detector thresholds. The gamma-flash backgrounds were approximated by decaying-exponential functions fitted in the regions which were equivalent to neutron energies above the maximum possible. The exponential extrapolation of the gamma flash was checked by examining data from runs using the CH<sub>2</sub> sample. For this sample the region corresponding to neutron energies greater than the maximum possible energy extends 3 MeV lower than that for <sup>16</sup>O because of the higher neutron separation energy in <sup>12</sup>C. Backgrounds from the sample container were measured directly and normalized to the foreground by examining regions where only aluminum photoneutrons were energetically allowed. The maximum systematic error introduced by these subtractions was 2.8%.

Time-of-flight spectra were then converted to neutron-energy spectra using the relation

$$E_n = m_0 c^2 \left[ \frac{1}{(1 - v_n^2/c^2)^{1/2}} - 1 \right], \quad (1)$$

where  $m_0$  is the rest mass of the neutron,  $c$  the speed of light, and  $v_n = L/t$  the speed of the neutron ( $L$  is the flight-path length and  $t$  is the neutron time of flight). The length of each flight

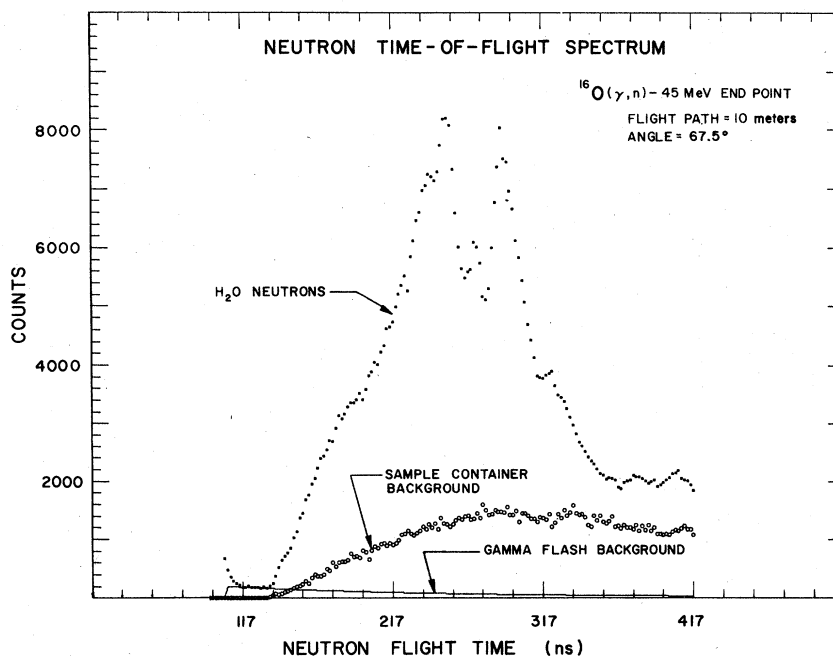


FIG. 3. Typical neutron time-of-flight spectrum, in this case, for the H<sub>2</sub>O sample at a 45-MeV end point and a 67.5° angle. Also shown are the background due to the aluminum sample container and the combined background due to gamma flash and time-independent sources.

path was accurately measured using a laser-ranging technique. Overall neutron-energy calibration (and consequently time calibration) was also tested comparing the graphite transmission data described above with the well-known carbon resonance energies.<sup>19</sup>

Relative detector efficiencies were measured by placing a small fission detector containing a  $^{252}\text{Cf}$  source at the sample position. The known neutron spectrum from  $^{252}\text{Cf}$  spontaneous fission<sup>20</sup> calibrated the relative efficiency of the detectors from threshold to approximately 8 MeV. In order to obtain the relative efficiencies at higher neutron energies, an analytical computer code<sup>21</sup> was used and normalized to the measured efficiencies. The efficiency code calculated contributions to the efficiency from elastic scattering including single, double, and triple scattering events for both hydrogen and carbon and from all inelastic processes (using the approximation of Ref. 22). Although the absolute efficiency obtained in this way could be in error by as much as 10%, the relative efficiency is most likely not in error by more than 2%.

After the neutron spectra were corrected for the detector efficiencies, the  $^{16}\text{O}$  data were converted to an excitation-energy scale (assuming that all neutrons left  $^{15}\text{O}$  in its ground state). To obtain absolute differential cross sections, these spectra must be corrected for the shape and magnitude of the incident photon spectrum for each end-point energy. This correction was derived from the  $\text{D}_2\text{O}$  spectra using the following procedure. The neutron spectrum from deuterium was determined by subtracting normalized  $\text{H}_2\text{O}$  spectra from the  $\text{D}_2\text{O}$  spectra. The normalization constant was determined from the data by requiring that structure in the neutron energy region of the  $^{16}\text{O}$  giant-dipole resonance and neutrons due to  $^{16}\text{O}$  at energies above the maximum allowed for deuterium both be canceled by the subtraction at all angles. The uncertainty in this normalization was determined from the scatter in the results from angle to angle to be at most 10%. After subtraction the resultant deuterium spectra were also converted to an excitation-energy scale. The shape of these spectra is a product of the photon flux and the deuterium cross section. To obtain the shape of the photon spectrum at each end-point energy, the deuterium cross section calculated by Partovi<sup>23</sup> was used. Finally the differential cross sections for  $^{16}\text{O}(\gamma, n_0)^{15}\text{O}$  were obtained by dividing the  $^{16}\text{O}$  spectra by the photon spectrum normalized by the constant used in subtracting the  $\text{H}_2\text{O}$  data from the  $\text{D}_2\text{O}$  data. The results are displayed in Fig. 4.

The differential cross sections as functions of excitation energy and center-of-mass angle then were fitted to a fourth-order Legendre polynomial

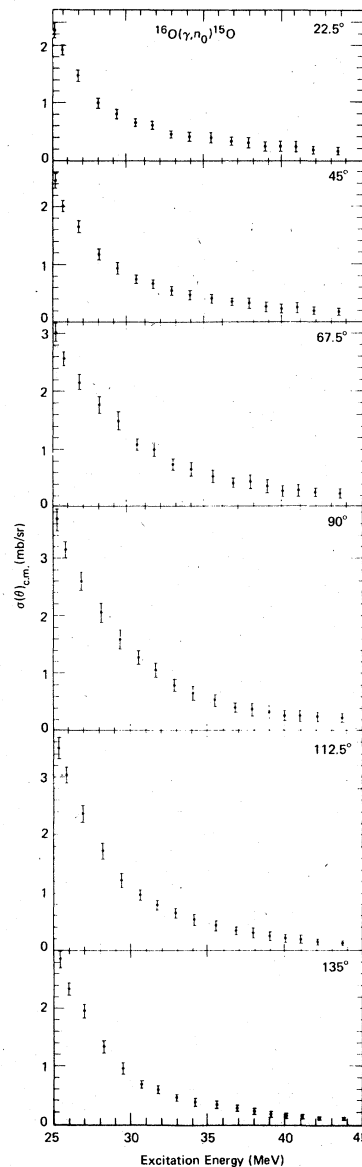


FIG. 4. Center-of-mass differential cross sections vs excitation energy for the  $^{16}\text{O}(\gamma, n_0)^{15}\text{O}$  reaction. (The angles labeling these cross sections are the laboratory angles.)

series,

$$\frac{d\sigma}{d\Omega}(E_x, \theta_{\text{c.m.}}) = \sum_{i=0}^4 a_i P_i(\cos\theta_{\text{c.m.}}), \quad (2)$$

where  $P_i(\cos\theta_{\text{c.m.}})$  are Legendre polynomials and  $a_i$  are the expansion coefficients. Since the first excited state of  $^{15}\text{O}$  is at 5.2 MeV, the uppermost 5 MeV of each end-point energy must indeed be due to ground-state transitions. Therefore collection of the highest 5 MeV from each end-point energy produced a ground-state cross section and angular distribution.

### III. RESULTS AND DISCUSSION

The cross section ( $4\pi a_0$ ) and the relative angular distribution coefficients ( $a_1/a_0$  through  $a_4/a_0$ ) are shown in Fig. 5. These results have been compiled from the four end-point energies that were examined in the present study. Although in principle only the highest 5 MeV of each of these end points was free of contamination by excited-state transitions, empirically all angular-distribution coefficients from a particular end point were in excellent agreement with the next lower end point for at least 4 MeV of their mutual overlap. In addition near the tip of each set of data statistical errors became very large, so that the highest 1–2 MeV of each end point has been deleted.

The error bars shown in Fig. 5 include counting-

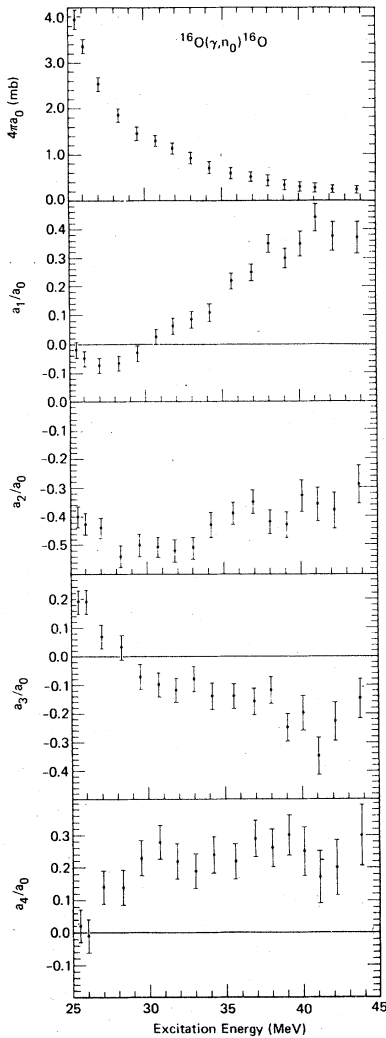


FIG. 5. Cross section ( $4\pi a_0$ ) and relative angular-distribution coefficients ( $a_i/a_0$ ) vs excitation energy for the  $^{16}\text{O}(\gamma, n_0)^{16}\text{O}$  reaction.

statistics errors, estimated errors in the angular-distribution fit, and a systematic error (which varied from angle to angle but was not greater than 4%) obtained from the estimates of error introduced by the various corrections to the data discussed in the previous section. Corroboration that the systematic errors did not exceed these estimates was derived from an angular-distribution fit to the deuterium data. Systematic deviations from the theoretical angular distribution in this case were used to estimate the systematic errors in the  $^{16}\text{O}$  angular distribution. The estimates using this method did not exceed the 4% quoted above. Not included in the error bars of  $4\pi a_0$  was an additional 20% systematic error primarily due to uncertainty in the normalization to deuterium and also small corrections for photon attenuation and neutron scattering in the sample.

In general the angular-distribution coefficients are smoothly varying with energy. Notice that  $a_1/a_0$  reaches a maximum value of approximately 0.4 at about 40 MeV and at the same energy  $a_3/a_0$  is approximately  $-0.25$ . Even more striking is the large positive  $a_4/a_0$  (approximately  $+0.25$  from 30 to 45 MeV). The appearance of large  $a_1/a_0$ ,  $a_3/a_0$ , and  $a_4/a_0$  coefficients is indicative of multipole absorption higher than  $E1$ . It is most probable that isovector electric-quadrupole absorption is the cause of these interference effects and the arguments supporting this conclusion are given below. However, it is appropriate to point out that such a conclusion will rest on several assumptions which can and should be checked by other experimental studies.

#### A. Detailed Analysis of the Angular Distribution Coefficients

If only  $E1$  and  $E2$  contributions to the cross section are included, there are four  $1p$ - $1h$  complex transition amplitudes to consider,  $s_{1/2}e^{i\phi_s}$ ,  $d_{3/2}e^{i\phi_d}$ ,  $p_{3/2}e^{i\phi_p}$ , and  $f_{5/2}e^{i\phi_f}$  where  $s_{1/2}$ , etc. are the real amplitudes and  $\phi_s$ , etc. are the real phase shifts. The angular distribution coefficients can then be expressed as functions of these eight variables,<sup>24</sup> i.e.,

$$a_0 = 0.75(s_{1/2}^2 + d_{3/2}^2) + 1.25(p_{3/2}^2 + f_{5/2}^2), \quad (3a)$$

$$a_1 = 2.372s_{1/2}p_{3/2}\cos(\phi_s - \phi_p) - 0.3354d_{3/2}p_{3/2}\cos(\phi_d - \phi_p) + 2.465d_{3/2}f_{5/2}\cos(\phi_d - \phi_f), \quad (3b)$$

$$a_2 = 1.061s_{1/2}d_{3/2}\cos(\phi_s - \phi_d) - 0.375d_{3/2}^2 + 0.625p_{3/2}^2 + 0.7143f_{5/2}^2 - 0.4374p_{3/2}f_{5/2}\cos(\phi_p - \phi_f), \quad (3c)$$

$$\begin{aligned}
a_3 = & 1.936s_{1/2}f_{5/2}\cos(\phi_s - \phi_f) \\
& + 2.012d_{3/2}p_{3/2}\cos(\phi_d - \phi_p) \\
& - 1.095d_{3/2}f_{5/2}\cos(\phi_d - \phi_f), \quad (3d)
\end{aligned}$$

$$a_4 = 3.499p_{3/2}f_{5/2}\cos(\phi_p - \phi_f) - 0.7143f_{5/2}^2. \quad (3e)$$

The  $s$  and  $d$  complex amplitudes arise from  $E1$  absorption while the  $p$  and  $f$  complex amplitudes arise from  $E2$  absorption. The assumption implicit in the above is that  $M1$ ,  $E3$ , and higher multipoles can be neglected. In the case of  $M1$ , analysis of  $(\vec{p}, \gamma_0)$  data has shown that neglecting  $M1$  in the GDR region (up to 27 MeV) is well justified.<sup>3</sup> Above the GDR the calculated  $M1$  cross section is at least a factor of 30 smaller than the  $E2$  cross section.<sup>17</sup> In the case of  $E3$ , again calculations<sup>13,15,17</sup> have shown that  $\sigma(E2)/\sigma(E3) \geq 80$ . Thus neglecting  $M1$ ,  $E3$ , and higher multipoles is probably justified.

In the five independent equations of Eqs. (3) there are eight variables. Since the phase shifts always appear as phase differences, one of these phase shifts can be arbitrarily fixed, i.e., take  $\phi_s = 0$ . In order to fully solve Eqs. (3) at least two of the remaining variables must be fixed, either by bringing in additional independent experimental evidence or by making some reasonable assumptions.

However, the primary interest here is to separate the  $E2$  cross section from the total, and the minimum and maximum  $E2$  cross section allowed by the angular distributions can be obtained without a solution for all variables. It is readily seen that in the expression for  $a_4/a_0$  the minimum values of  $p_{3/2}$  and  $f_{5/2}$  will occur when  $\cos(\phi_p - \phi_f) = 1$ . The minimum  $E2$  cross section is easily found (by minimizing  $p_{3/2}^2 + f_{5/2}^2$  in  $a_4/a_0$  and  $a_0$ ) to be given by

$$\sigma(E2)_{\min} = \frac{7}{2}\pi a_4. \quad (4)$$

To obtain the maximum  $E2$  cross section, the  $E1$  cross section must be minimum and it can be seen that the minimum value of  $s_{1/2}^2 + d_{3/2}^2$  will occur in the expression for  $a_2/a_0$  when  $\cos(\phi_s - \phi_d) = -1$ . Then by using  $a_4/a_0$ ,  $a_2/a_0$ , and  $a_0$  and minimizing  $s_{1/2}^2 + d_{3/2}^2$  the maximum  $E2$  cross section is given in this case by

$$\sigma(E2)_{\max} = \frac{2}{3}\sigma_0 + \frac{8}{3}\pi(a_2 + a_4), \quad (5)$$

where  $\sigma_0$  is the total measured cross section.

The results of Eqs. 4 and 5 are shown in Fig. 6 where the appropriate extremes in the error bars of the angular-distribution coefficients were used in calculating these curves. The rather narrow limits placed on the  $E2$  cross section are primarily a consequence of the large  $a_4/a_0$  coefficient ob-

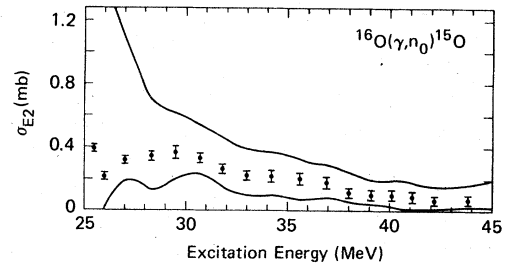


FIG. 6. Electric-quadrupole cross section vs excitation energy for the  $^{16}\text{O}(\gamma, n_0)^{15}\text{O}$  reaction. The solid lines are upper and lower limits on this cross section based on the present data alone. The data points were obtained by including information from polarization measurements (see text).

tained here.

Below an excitation energy of approximately 30 MeV, the polarization of the photoneutrons has been measured at  $45^\circ$  and  $90^\circ$  (Ref. 25). These measurements provide the required two additional equations necessary to solve for all eight variables of Eqs. (3). Fortunately, this occurs at just the energies where the limits on the  $E2$  cross section are becoming very wide. Furthermore, the analysis of the  $(\vec{p}, \gamma_0)$  data of Ref. 3 can provide at least a starting point for obtaining a solution to Eqs. (3) augmented by the polarization information. In this analysis a remarkable constancy of the  $s_{1/2}$  to  $d_{3/2}$  amplitudes and of the  $(\phi_s - \phi_d)$  phase difference over the GDR region was found. In the present analysis it was found that values of  $s_{1/2}/d_{3/2}$  and  $(\phi_s - \phi_d)$  very close to those of Ref. 3, specifically 0.75 and approximately  $-120^\circ$  respectively (the two solutions of Ref. 3 agree within errors in this energy region), were able to satisfy both the present angular distributions and the polarizations [ $P_n(45^\circ) = 0.45 \pm 0.1$  at 25 MeV decreasing to  $0.30 \pm 0.1$  at 30 MeV and  $P_n(90^\circ) = -0.05 \pm 0.1$  at 25 MeV increasing to  $0.15 \pm 0.1$  at 30 MeV]. Above 30 MeV where there are no polarization measurements the following assumptions were made: The ratio of  $s_{1/2}$  to  $d_{3/2}$  was assumed to be constant at 0.75 and the  $(\phi_s - \phi_d)$  phase difference was allowed to vary such that  $P_n(45^\circ)$  and  $P_n(90^\circ)$  varied slowly by not more than  $\pm 0.20$  from their values at 30 MeV.

The  $E2$  cross section calculated from the solutions obtained above are also shown in Fig. 6. Below 30 MeV the calculated  $E2$  cross section depends only on the reliability of the measured angular distributions and polarizations. Above 30 MeV the assumptions made above are critical and can only be verified by a measurement of the polarization (for at least two angles). However, the limits on the  $E2$  cross section in this region are fairly narrow and the calculated  $E2$  cross section

is at least reasonable. The error bars in Fig. 6 reflect only the errors on the angular-distribution coefficients.

It is very difficult to identify the resonant structures which make up this  $E2$  cross section for several reasons including the assumptions necessary to calculate the cross section, the expected large width of resonances at these excitation energies, and the relatively poor resolution at these energies (1.3 MeV at 35 MeV). Nevertheless, one can speculate that there may be a resonance centered at about 29 MeV with a width of 4–5 MeV and a very broad ( $\sim 7$ -MeV) resonance at approximately 35 MeV. In any case the energy-weighted integration of the  $E2$  cross section gives  $3.8 \pm 1.2 \times 10^{-3}$  mb/MeV for the  $(\gamma, n_0)$  channel which is 68% of the energy-weighted sum rule EWSR (Ref. 16) for isovector  $E2$  which for the neutron channel is given by

$$\text{EWSR}_1 = \frac{dE_\gamma \sigma(E_\gamma)}{E_\gamma^2} = \frac{5}{4\pi} \frac{\hbar^2 NZ}{M A} \langle \gamma^2 \rangle \quad (6)$$

(where  $\langle \gamma^2 \rangle$  is taken as  $0.6 R^2$  where  $R$  is the radius of the uniform mass distribution given by  $R = 1.2 A^{1/3}$  fm). Note that the energy-weighted integration of the lower-limit cross section is 31% of the EWSR<sub>1</sub>.

The primary evidence that the  $E2$  cross section measured here is isovector is its high excitation energy. However, approximately one isoscalar EWSR has been exhausted at lower excitation energies. The  $(\gamma, \alpha_0)$  channel<sup>2</sup> which must be isoscalar exhausts at least 55% of the EWSR<sub>0</sub> and the  $(\gamma, p_0)$  channel<sup>3</sup> which has been interpreted as isoscalar exhausts up to 70% of the EWSR, below 27 MeV. In the latter case part of the measured cross section at the higher excitation energies may be isovector just as in the present measurement part of the cross section at the lower excitation energies may be isoscalar. The  $E2$  cross section for the other major reaction channel,  $(\gamma, n_0)$ , has not been measured in detail below 25 MeV but is estimated<sup>26</sup> to be of the same order as the  $(\gamma, p_0)$  cross section.

#### B. Comparison with Other Experimental Results

All of the previous photoneutron and most of the previous photoproton (or equivalently the inverse proton capture) experiments have not investigated the energy range of 30–50 MeV. In Fig. 7 the present data are compared to a selection of the existing angular distribution data.

In the small region of overlap between the present data and the earlier photoneutron data of Jury *et al.*<sup>26</sup> (where the last 1.0 MeV of these data has been deleted since they are unreliably close to the end point), there is good agreement in  $a_3/a_0$  and

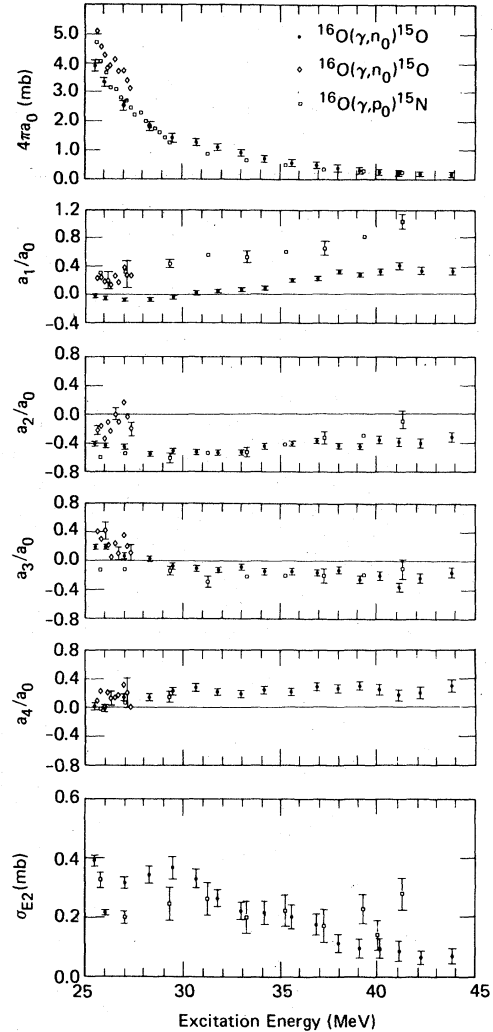


FIG. 7. Comparison of the present results (solid circles) for the  $^{16}\text{O}(\gamma, n_0)^{15}\text{O}$  reaction with the results of Ref. 26 (open diamonds) for the same reaction and with the results of Refs. 8 and 9 (open squares) for the  $^{16}\text{O}(\gamma, p_0)^{15}\text{N}$  reaction [obtained from  $^{13}\text{N}(p, \gamma_0)^{16}\text{O}$  data by detailed balance].

$a_4/a_0$  and fair agreement in  $a_1/a_0$  and  $a_2/a_0$ . Recently this lower energy photoneutron experiment was repeated at the NRCC Laboratory in Ottawa<sup>27</sup> with very nearly the same results as here and in Ref. 26. Even more interesting is the comparison between the present data and the proton capture data of Ref. 8 since these data cover the same energy-range. The shapes of all angular distribution coefficients ( $a_4/a_0$  was not reported in Ref. 8) are nearly the same throughout. The magnitude of  $a_2/a_0$  is also the same, but  $a_1/a_0$  is about 0.15 lower, and  $a_3/a_0$  is 0.2 higher on the average in the proton capture case. Tentative results from a proton-capture measurement at this laboratory<sup>10</sup> are near-

ly the same as those of Ref. 8, but the measured  $a_4/a_0$  has a small negative value. However, there is good agreement between the  $E2$  cross sections deduced from the present data and the data of Ref. 8 as shown in Fig. 7(f) where in the latter case the  $\sigma(E2)$  was determined from  $a_1/a_0$  and  $a_3/a_0$  by the method described in Ref. 28. From this it can be concluded that the  $p$  and  $f$  amplitudes must be nearly the same in the  $(\gamma, p_0)$  and  $(\gamma, n_0)$  reactions, but the phases may be quite different.

The only other experimental result which finds evidence for higher order multipole absorption in the 30–50 MeV region is the polarized-proton elastic-scattering measurement of Geramb *et al.*<sup>12</sup> Although in this measurement these authors find evidence for  $E2$  and even  $E3$  strength, there apparently are difficulties in converting their experimental coupling constants to cross sections. Consequently detailed comparisons cannot be made.

Finally in Fig. 8 the results of several cross section measurements in the 25–45 MeV range are illustrated. Included in this figure are the present  $(\gamma, n_0)$  data, the  $(\gamma, p_0)$  data [obtained by the inverse  $(p, \gamma_0)$  reaction] of Refs. 8 and 9, the total-neutron cross section data of Ref. 29, and the total-absorption cross section data of Ref. 30. In the case of the total-neutron cross section which is composed of  $\sigma(\gamma, n) + \sigma(\gamma, np) + \sigma(\gamma, 2n) + \dots$  Veyssi re *et al.*<sup>31</sup> obtained results similar to Ref. 30 but were also able to separately measure  $\sigma(\gamma, np)$  and  $\sigma(\gamma, 2n)$ . They show that  $\sigma(\gamma, np) + \sigma(\gamma, 2n)$  reaches an approximately constant value

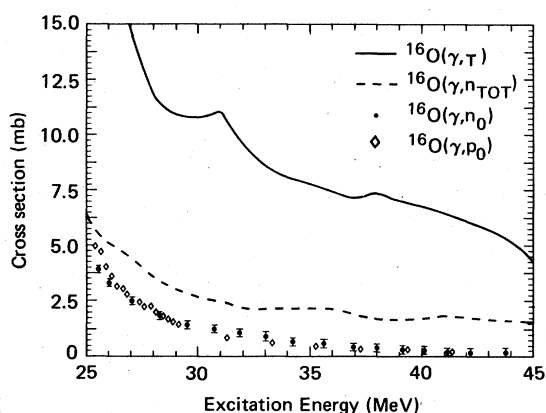


FIG. 8. Comparison of the cross section for the  $^{16}\text{O}(\gamma, n_0)^{15}\text{O}$  reaction (solid circles) obtained here with the total-absorption cross section for  $^{16}\text{O}$  (solid line) from Ref. 30, the total-neutron cross section for  $^{16}\text{O}$  (dashed line) from Ref. 29, and the cross section for the  $^{16}\text{O}(\gamma, p_0)^{15}\text{O}$  reaction (open diamonds) from Refs. 8 and 9 [obtained from  $^{15}\text{N}(p, \gamma_0)^{16}\text{O}$  data by detailed balance].

of nearly one half the total-neutron cross section at about 31 MeV. Consequently  $\sigma(\gamma, n)$  is only slightly larger than  $\sigma(\gamma, n_0)$ . This result correlates very well with the observation here that there is a high degree of overlap between the higher end-point spectra and the lower end points (i.e., small cross sections for leaving  $^{15}\text{O}$  in an excited state).

### C. Comparison with Theoretical Results

As discussed in the Introduction there are several microscopic calculations which include  $E2$  and higher multipole absorption and cover the energy range examined here.<sup>13-18</sup> Among these, the studies by Marangoni *et al.*<sup>15</sup> and Heil<sup>17</sup> predict partial cross sections and angular distributions. Both calculations use the coupled-channel model with a  $1p-1h$  basis in the Tamm-Dancoff approximation. In addition, the calculation of Ref. 16 uses the separation approximation of the energy and radial dependence of the single-particle continuum functions developed by Birkholz.<sup>32</sup> In Fig. 9

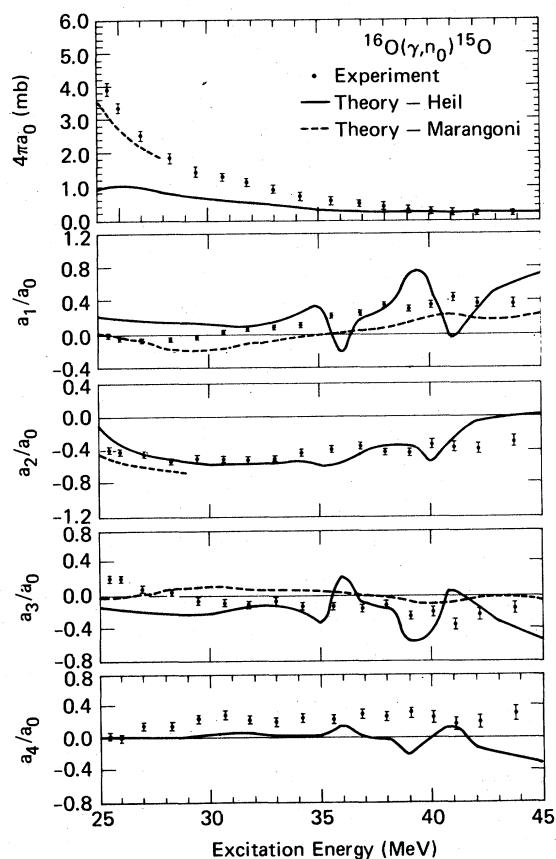


FIG. 9. Comparison of the present results (solid circles) for the  $^{16}\text{O}(\gamma, n_0)^{15}\text{O}$  reaction with the theoretical results of Ref. 17 (solid line) and Ref. 15 (dashed line).

the results of these calculations are compared to the present data. While these calculations reproduce the trend of the data, the overall agreement is not very good. Especially disturbing are the sharp fluctuations in the angular distribution coefficients of Ref. 17. At these high excitation energies any resonant structure is expected to be quite broad. Note that to obtain the theoretical results, a renormalization of the  $E1$  amplitudes was performed in Ref. 17 while in Ref. 15 an imaginary part was added to the single-particle potential.

Although Marangoni *et al.*<sup>15</sup> calculate an  $E2$  cross section for the  $(\gamma, n_0)$  reaction, it is at least four times smaller than the cross section obtained in this experiment. It is difficult to suggest which aspects of these theoretical studies should be investigated in order to improve the agreement with the theoretical results. However, the present data do provide a necessary test for any further theoretical studies.

Another important theoretical investigation of giant-multipole resonances is that of Liu and Brown.<sup>16</sup> In this study the authors use the random-phase approximation based on a Hartree-Fock ground-state calculated with a Skyrme type interaction. The isoscalar and isovector quadrupole strengths are calculated separately. Strong isovector quadrupole strength is predicted at 26.5, 31, 33, and 37 MeV, along with weak isoscalar strength in this same 25 to 40 MeV region. Although these results compare favorably with the present data, more detailed theoretical predictions (i.e., the complex amplitudes of emitted nucleons are necessary before stronger conclusions can be drawn. The same remark is applicable to the remaining theoretical studies cited.<sup>5,13,14,18</sup>

Before closing this section, mention should be made of the hydrodynamic model which has had remarkable success in predicting the location of giant resonances (especially in medium-weight and heavy nuclei). In this model the isovector  $E2$  giant resonance is predicted at an energy given by  $130 A^{-1/3}$  MeV (Ref. 33) which for  $^{16}\text{O}$  is 51.6 MeV. Although the experimental result of 30–40 MeV is somewhat lower than this prediction, the giant  $E1$  resonance is also experimentally found to be sys-

tematically lower than the hydrodynamic model prediction in light nuclei.

#### IV. CONCLUSIONS

The photoneutron cross section and angular distribution for the reaction  $^{16}\text{O}(\gamma, n_0)^{15}\text{O}$  have been measured over the excitation energy range of 25 to 45 MeV. Angular distributions were fitted to a fourth-order Legendre-polynomial expansion. The large value of the  $a_4/a_0$  coefficient over most of this energy range (0.25 between 30 and 45 MeV) provides strong evidence for a sizable  $E2$  cross section. Using the present data and previous photoneutron-polarization measurements, an  $E2$  cross section was extracted. Although not definitive, the shape of this cross section is consistent with at least two resonances at approximately 29 and 35 MeV. The energy-weighted integral of the  $E2$  cross section exhausts 68% of the isovector energy-weighted sum rule. Because the isoscalar EWSR has been exhausted at lower energies and simply because of the high excitation energies investigated here, this cross section most likely is isovector  $E2$ . However, the presence of some isoscalar  $E2$  strength cannot be ruled out.

Good agreement is seen in the comparison between the present results and previous  $(\gamma, n_0)$  measurements and  $(\gamma, p_0)$  measurements [through the inverse  $(p, \gamma_0)$  reaction]. Especially interesting is the comparison with the latter reaction. Although the angular-distribution coefficients have nearly the same energy dependence, there apparently is a systematic difference in the magnitudes. However, when the  $E2$  cross sections are extracted from both sets of data, nearly the same result is obtained. The conclusion is that the real part of the complex amplitudes must be almost the same while the phases are systematically different.

All the microscopic theoretical studies on  $^{16}\text{O}$  predict strong isovector  $E2$  absorption in the 30–40 MeV region in good agreement with the present results. However, in those investigations in which partial cross sections and angular distributions were calculated, the detailed agreement with the present data is not especially good. The present results provide a needed benchmark for further theoretical investigations of higher multipole resonances in this nucleus.

\*Permanent address: Department of Physics, The Pennsylvania State University, Delaware County Campus, Media, Pennsylvania 19063.

<sup>1</sup>S. S. Hanna, in *International School on Electro- and Photonicuclear-Reactions, Erice, Italy, 1976*, edited by S. Costa and C. Schaerf (Springer, Berlin, 1977),

Vol. I, pp. 275–339.

<sup>2</sup>K. T. Knöpfle, G. J. Wagner, H. Breuer, M. Rogge, and C. Mayer-Böricke, *Phys. Rev. Lett.* **35**, 779 (1975); M. N. Harakeh, A. R. Arends, M. J. A. DeVoight, A. G Drentje, and S. Y. Van der Woude, *Nucl. Phys.* **A265**, 189 (1976); K. A. Snover, E. G. Adel-

- berger, and D. R. Brown, Phys. Rev. Lett. 32, 1061 (1974); K. T. Knopfle, G. J. Wagner, P. Paul, H. Breuer, C. Mayer-Boricke, M. Rogge, and P. Turek, Phys. Lett. 74B, 191 (1978).
- <sup>3</sup>S. S. Hanna, H. F. Glavish, R. Avida, J. R. Calarco, E. Kuhlmann, and R. La Canna, Phys. Rev. Lett. 32, 114 (1974); R. La Canna, H. F. Glavish, J. R. Calarco, and S. S. Hanna, Progress Report (Department of Physics, Stanford University, Stanford, 1975), p. 42.
- <sup>4</sup>A. Hotta, K. Itoh, and T. Saito, Phys. Rev. Lett. 33, 790 (1974).
- <sup>5</sup>T. T. S. Kuo and E. Osnes, Phys. Lett. 42B, 335 (1972).
- <sup>6</sup>D. E. Frederick, R. J. J. Stewart, and R. C. Morrison, Phys. Rev. 186, 992 (1969).
- <sup>7</sup>S. H. Chew, J. Lowe, J. M. Nelson, and A. R. Barnett, Nucl. Phys. A286, 451 (1977).
- <sup>8</sup>P. Paul, J. W. Noe, K. A. Snover, M. Suffert, E. K. Warburton, and H. M. Kuan, in *International Symposium on Highly Excited States in Nuclei, Julich, 1975*, edited by A. Faessler, C. Mayer-Boricke, and P. Turek, Proceedings, Vol. 1, p. 2.
- <sup>9</sup>W. J. O'Connell and S. S. Hanna, Phys. Rev. C 17, 892 (1978).
- <sup>10</sup>F. S. Dietrich, private communication.
- <sup>11</sup>J. M. Eisenberg and W. Greiner, in *Nuclear Theory Vol. 2 (Excitation Mechanisms of the Nucleus)* (North-Holland, Amsterdam, 1970), p. 98.
- <sup>12</sup>H. V. Geramb, R. Sprickmann, and G. L. Strobel, Nucl. Phys. A199, 545 (1973); D. Lebrun, G. Perrin, P. Martin, P. De Saintignon, J. Arvieux, M. Buenerd, H. V. Geramb, and K. A. Amos, *ibid.* A265, 291 (1976).
- <sup>13</sup>S. Krewald, J. Birkholz, A. Faessler, and J. Speth, Phys. Rev. Lett. 33, 1386 (1974).
- <sup>14</sup>S. Shlomo and G. Bertsch, Nucl. Phys. A243, 507 (1975).
- <sup>15</sup>M. Marangoni, P. L. Ottaviani, and A. M. Saruis, Report CNEN RT/FI (76) 10 (1976).
- <sup>16</sup>K. F. Liu and G. E. Brown, Nucl. Phys. A265, 385 (1976).
- <sup>17</sup>V. Heil, Ph.D. thesis (Technische Hochschule Darmstadt, Darmstadt, 1977).
- <sup>18</sup>J. S. Dehesa, S. Krewald, J. Speth, and Amand Faessler, Phys. Rev. C 15, 1858 (1977).
- <sup>19</sup>D. B. Fossan, R. L. Walton, W. E. Wilson, and H. H. Barschall, Phys. Rev. 123, 209 (1961).
- <sup>20</sup>A. Koster, in *Prompt Fission Neutron Spectra, Vienna, 1971* (International Atomic Energy Agency, Vienna, 1972), p. 19.
- <sup>21</sup>B. Ripin, Rensselaer Polytechnic Institute Report (RPI, Troy, New York, 1964).
- <sup>22</sup>H. L. Anderson, E. P. Hincks, C. S. Johnson, C. Rey, and A. M. Segar, Phys. Rev. 133, B396 (1964).
- <sup>23</sup>F. Partovi, Ann. Phys. (N. Y.) 27, 29 (1964).
- <sup>24</sup>R. W. Carr and J. E. E. Baglin, Nucl. Data Tables 10, 143 (1971).
- <sup>25</sup>F. A. Hanser, Ph.D. thesis (M.I.T., Cambridge, 1967), G. W. Cole Jr., F. W. K. Firk, and T. W. Phillips, Phys. Lett. 30B, 91 (1969); R. Nath, F. W. K. Firk and H. L. Schultz, Nucl. Phys. A194, 49 (1972).
- <sup>26</sup>J. W. Jury, J. S. Hewitt, and K. G. McNeill, Can. J. Phys. 48, 1635 (1970).
- <sup>27</sup>J. W. Jury, private communication.
- <sup>28</sup>K. A. Snover, K. Ebisawa, D. R. Brown, and P. Paul, Phys. Rev. Lett. 32, 317 (1974).
- <sup>29</sup>U. Kneissl, E. A. Koop, G. Kuhl, K. H. Leister, and A. Weller, Nucl. Instrum. Methods 127, 1 (1975).
- <sup>30</sup>J. Ahrens, H. Borchert, K. H. Czock, H. B. Eppler, H. Gimm, H. Gundrum, M. Kröning, P. Riehn, G. Sita Ram, A. Zeigler, and B. Zeigler, Nucl. Phys. A251, 479 (1975).
- <sup>31</sup>A. Veyssière, H. Beil, R. Bergère, P. Carlos, A. Leprêtre, and A. de Miniac, Nucl. Phys. A227, 513 (1974).
- <sup>32</sup>J. Birkholz, Nucl. Phys. A189, 385 (1972); J. Birkholz, Phys. Lett. 34B, 1 (1971).
- <sup>33</sup>B. R. Mottelson, in *Proceedings of the International Conference on Nuclear Structure, Kingston, 1960*, edited by D. A. Bromley and E. W. Vogt (University of Toronto Press, Toronto/North-Holland, Amsterdam, 1960); A. Bohr, in *Nucl. Physics: An International Conference*, edited by R. Becker, C. Goodman, P. Stelson, and A. Zucker (Academic, New York, 1967).